Nano World Journal

https://doi.org/10.17756/nwj.2022-s1-010

Research Article

Open Access

Improvement in the Material Properties of Hydrothermally Synthesized WS_2 with Increased Drying Temperature

Prarbdh Bhatt[1], Vipin Kumar[2], Moti Kumar Jha[3], and Nilanjan Halder[1*]

[1]*Department of Physics, Manipal University Jaipur, India*

[2]*Department of Physics, Yeungnam University, Gyeongsan, Gyeongbuk, South Korea*

[3]*Sophisticated Analytical Facility, Manipal University Jaipur, India*

***Correspondence to:**
Nilanjan Halder
Department of Physics, Manipal University Jaipur, India
E-mail: nhalder2@yahoo.com

Received: August 23, 2022
Accepted: October 13, 2022
Published: October 15, 2022

Citation: Bhatt P, Kumar V, Jha MK, Halder N. 2022. Improvement in the Material Properties of Hydrothermally Synthesized WS_2 with Increased Drying Temperature. *Nano World J* 8(S1): S49-S53.

Copyright: © 2022. Bhatt et al. This is an Open Access article distributed under the terms of the Creative Commons Attribution 4.0 International License (CC-BY) (http:// creativecommons.org/licenses/by/4.0/) which permits commercial use, including reproduction, adaptation, anddistribution of the article provided the original author and source are credited.

Published by United Scientific Group

Abstract

Tungsten disulfide (WS_2) is one of the most promising alternatives of 2D materials because of its bandgap energy, excellent electrical, and optoelectronic properties. The enhanced carrier confinement due to reduced lateral size of the WS_2 quantum dots (QDs) make them promising for applications like bio-imaging and photocatalysis. The WS_2 QDs generally emit in the blue region of the visible light spectrum.We have prepared bulk WS_2 by a facile solution based hydrothermal technique. The as-prepared bulk material is dried at 60 °C and 80 °C temperatures with varied dwelling time to get powder WS_2 with improved crystal properties. The physical properties of the dried powder material were investigated by different techniques like X-ray diffraction (XRD) and Fourier transform infrared spectroscopy (FTIR) to understand the improvement in the crystal property of the material with drying temperature. Further, WS_2 QDs were produced by mechanically exfoliating the WS_2 bulk and the tunable bandgap of the QDs with drying temperature was investigated by Ultraviolet-Visible (UV-Vis) spectroscopy. Photoluminescence (PL) from the WS_2 QDs with optimized physical properties was also measured to comment on the excitonic behavior of the nanostructures.

Keywords

Tungsten disulfide, Quantum dots, Crystal property evolution, Photoluminescence spectroscopy

Introduction

One of the most promising transition metals dichalcogenides (TMDCs) is WS_2 owing to light emission in the monolayer form at ~2 eV and the low level of toxicity of the synthesis processes [1]. WS_2 have attracted a huge attention due to its unique and fascinating physical properties, such as, bandgap energy, excellent electrical and optoelectronic properties, etc. The relatively high carrier mobility, large exciton binding energy, large spin orbit splitting, and strong photoluminescence makes the material useful for applications like photodetectors, spin-valley transistors, LEDs, etc. [2-4]. WS_2 QDs show enhanced carrier confinement due to reduced lateral size and have their applications in bio imaging and photocatalysis. The WS_2 QDs generally emit in the blue region of the visible light spectrum and the quantum confinement, edge effects, and structural defects govern their tunable optical properties. Besides an efficient and scalable synthesis method, a well optimized post synthesis processing recipe is required to be developed for obtaining good crystal quality nanostructured WS_2. While the former is well established and has been reported in literature [5], the latter requires a comprehensive study.

We have prepared bulk WS_2 by a facile solution based hydrothermal technique. The as-prepared bulk material was dried at different temperatures (less than 100 °C) with different dwelling times to get powder WS_2 with improved crystal properties. The physical properties of the dried powder material were investigated by techniques like XRD and FTIR Further, QDs like nanostructured WS_2 was fabricated by mechanically exfoliating the WS_2 bulk and evolution of the tunable optical property of the QDs with drying temperature was investigated by UV-Vis spectroscopy. PL from the WS_2 QDs with optimized physical properties was also measured to investigate the excitonic properties of the nanostructures.

Materials and Methods

In this work, we have fabricated WS_2 nanoparticles by a facile one step hydrothermal method. The starting materials were Tungsten hexachloride (WCl_6) and Thioacetamide (TAA). The ratio WCl_6:TAA was chosen in such a way to get phase pure bulk WS_2 [6]. The starting materials weredispersed in ethanol and stirred for 1 hour under ambient room temperature. The dispersed reactants were then kept in a hydrothermal reactor with Teflon lined vessel at 180 °C for 24 hours. Once cooled, the products of the hydrothermal synthesis were then filtered out and the dark colored residue was washed thoroughly with deionized (DI) water. The properly washed residue was then dried inside a hot air oven at 60 °C and 80 °C temperatures with dwelling time of 3 and 24 hours. The drying process also ensures sublimation of the compounds adsorbed in the material during the facile synthesis and was expected to improve the crystal quality of the synthesized bulk powder.

For producing WS_2 QDs, a few mg of dark colored precipitate was further dispersed in NMP N-Methyl-2-pyrrolidone (NMP) and probe sonicated for 4 hours at 500 W to exfoliate mechanically. Finally, the exfoliated solution was centrifuged at 5500 rpm and the supernatant was collected for characterization.

Rigaku X-ray diffractometer (SMARTLAB) was used for structural characterization of the samples. Field emission scanning electron microscopy (FESEM) imaging of the dried samples was carried out using JEOL FESEM (JSM-7610FPlus) and the IR spectra of the samples was investigated using FTIR (Bruker ALPHA) spectrometer. Size of the WS_2 QDs dispersed in NMP was measured using Anton Paar (Litesizer 500) Dynamic Light Scattering (DLS) system. Bandgap of the WS_2 QDs was determined by measuring the optical absorption with UV-Vis spectrophotometer (Shimadzu UV-2600). Horiba (FluoroMax-4) spectrometer was used to study the PL emission from the nanostructured QDs.

Results and Discussion

The XRD pattern of the samples dried at different temperatures (60 °C and 80 °C) with varied dwelling times was displayed in Figure 1. In the Figure 1, the peaks at 31°, 35°, 42°, and 56° are assigned due to diffraction from the (100), (102), (006), and (110) planes of the hexagonal phase of WS_2 (JCPDS Card No.00-008-0237) [7]. Moreover, a XRD

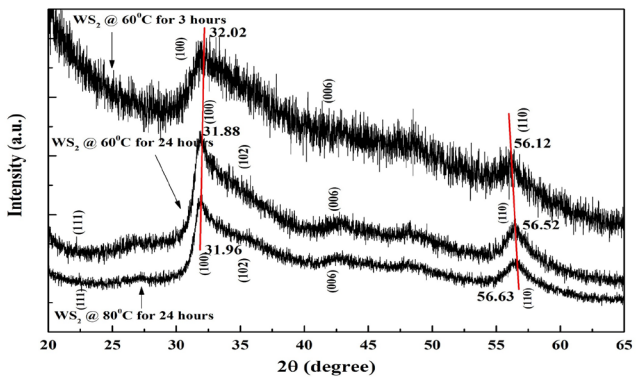


Figure 1: The XRD pattern of the dried samples.

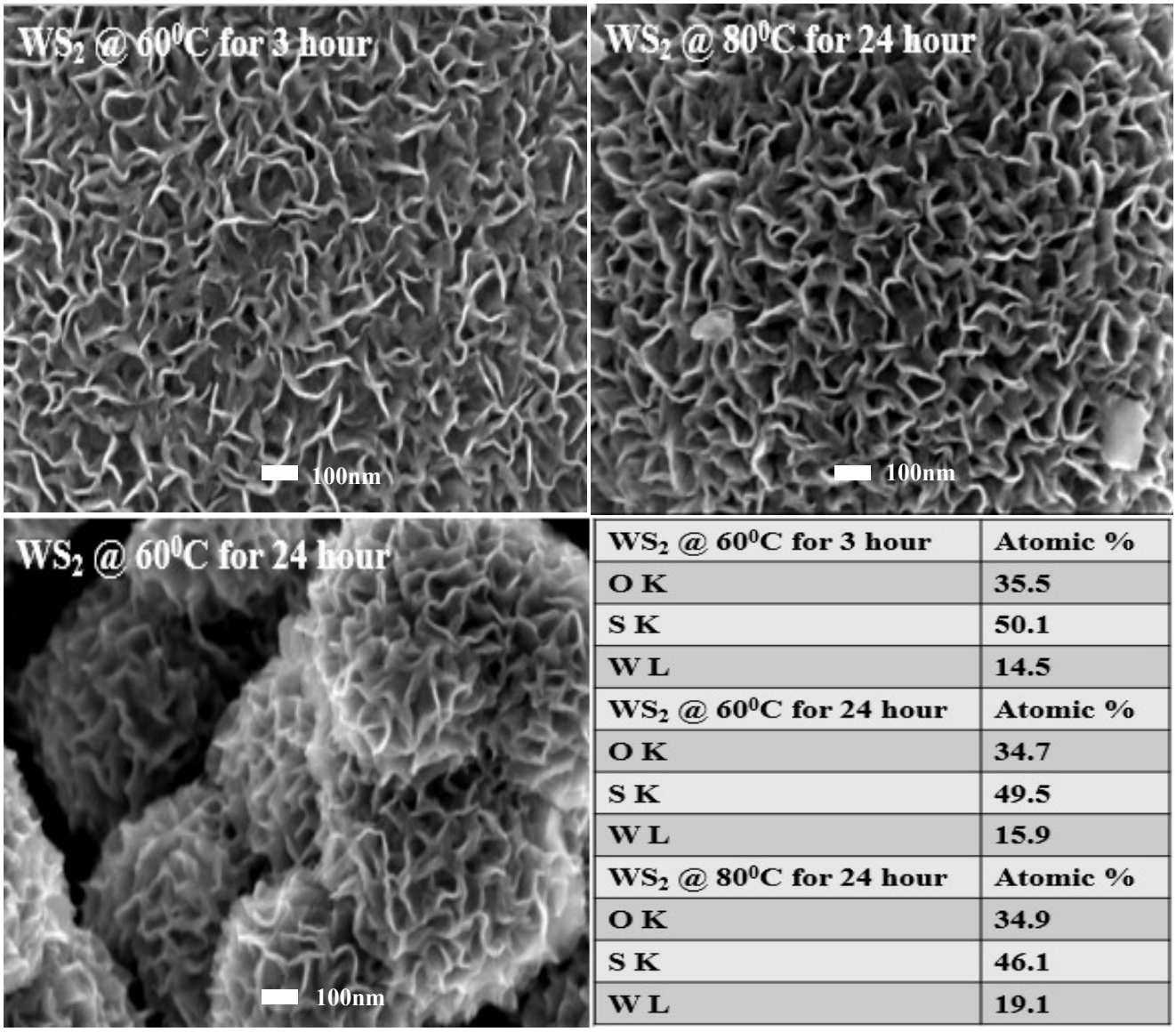
peak at 23° corresponding to the (111) plane of WO_3 can also be observed in the samples dried at 60 °C and 80°C for 24 hours, which agrees with the high susceptibility of WS_2 to be oxidized at the defective edge planes at elevated temperatures [7]. The emergence of secondary WO_3 phase due to annealing of WS_2 has been reported in literature [8]. The prominence of the XRD peaks with the increase of the drying time and drying temperature suggests the amorphous to crystalline state transformation of the synthesized WS_2 powder bulk. Further, shifting of the Bragg peaks can also be observed from the XRD data. The shift indicates a change in the lattice parameter due to crystallinity change of the WS_2 bulk with drying temperature and drying time.

The FESEM images shown in Figure 2, confirm that the microstructures of the samples consist of intertwined WS_2 nanosheet aggregates. The Energy-dispersive X-ray spectroscopy (EDS) analysis of the sample shown in the Figure 2, displaying the atomic percentage of W, S and O elements, confirms the elemental composition of the samples.

The vibrational modes present in the WS_2 samples subjected to post synthesis drying have been investigated using FTIR spectroscopy technique. The FTIR data from the samples (Figure 3) are consistent with the previously published results of WS_2 and WO_3 [9-11]. The only difference between the spectra was the omission of the peak at 1098 cm^{-1} in the sample being dried at 80 °C for 24 hours. The 1098 cm^{-1} peak, which has its existence only in the WS_2 samples dried at 60 °C for 3 hours and 24 hours, was reported to be due to S-S bond in WS_2 and indicates considerable Sulphur content at the surface of the samples [9].

The DLS spectra (Figure 4a) of the solvent dispersed WS_2 QDs, produced by mechanical exfoliation of the dried WS_2 sample in NMP solvent, reveals that the QDs sizes were of the order of 1 nm. The 25% polydispersity index of the QDs sample as measured by DLS experiment indicates good size uniformity of the sample.

The UV-Vis spectra of the solution dispersed QDs, displayed in Figure 4(b)-4(d), shows that the solution dispersed QDs were having the highest optical absorption in the UV region around 300 nm. The direct bandgap energy of the QDs was estimated from the well-known Tauc's equation considering direct transition of the electrons from the conduction to the valence band [12]. The Tauc's plots were displayed in



WS_2 @ 60°C for 3 hour	Atomic %
O K	35.5
S K	50.1
W L	14.5
WS_2 @ 60°C for 24 hour	Atomic %
O K	34.7
S K	49.5
W L	15.9
WS_2 @ 80°C for 24 hour	Atomic %
O K	34.9
S K	46.1
W L	19.1

Figure 2: The FESEM image and EDS analysis of the samples dried at 60 °C and 80 °C with varied dwelling time 3 hours and 24 hours.

the inset of the Figure 4(b)-4(d). The QDs exhibited a blue shift in the direct band gap energy with drying temperature and drying time. As seen in the XRD data, the WS_2 samples undergo a transformation from amorphous to crystalline state when subjected to drying at elevated temperature for longer time. The phase transformation was associated with desulphurization of the material at the edge planes promoting the formation of WO_3 phase thereby, resulting a change in the lattice constant and crystal structure of the material [7]. The change in the crystal structure affects the K point in the Brillouin zone of the material, which can be ascribed to be the primary cause for the blueshift in bandgap energy of the WS_2 QDs with drying temperature and drying time.

Finally, we have investigated the excitonic properties of the QDs produced from the WS_2 sample dried at 80 °C for 24 hours. As revealed from the XRD patterns, the sample dried at 80 °C was of best quality in terms of crystalline structure. The room temperature PL spectra of the sample shown in Figure 5 can be deconvoluted into four characteristic peaks. The first two peaks can be assigned due to B excitonic (360 nm) and A excitonic (409 nm) transitions in the samples. The strong excitonic binding energies as a result of reduced dielectric screening in 2D TMD material promote the formation of

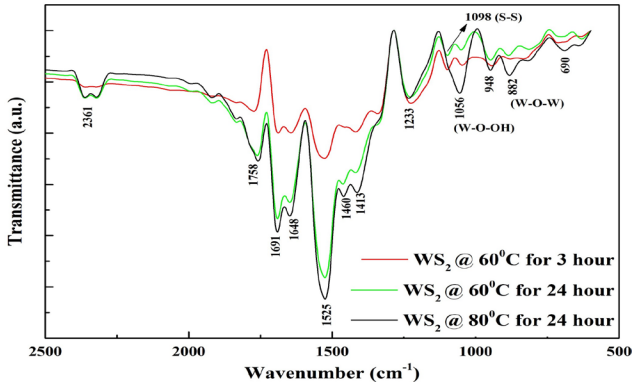


Figure 3: The FTIR spectra of the samples dried at 60 °C and 80 °C 3 hours and 24 hours.

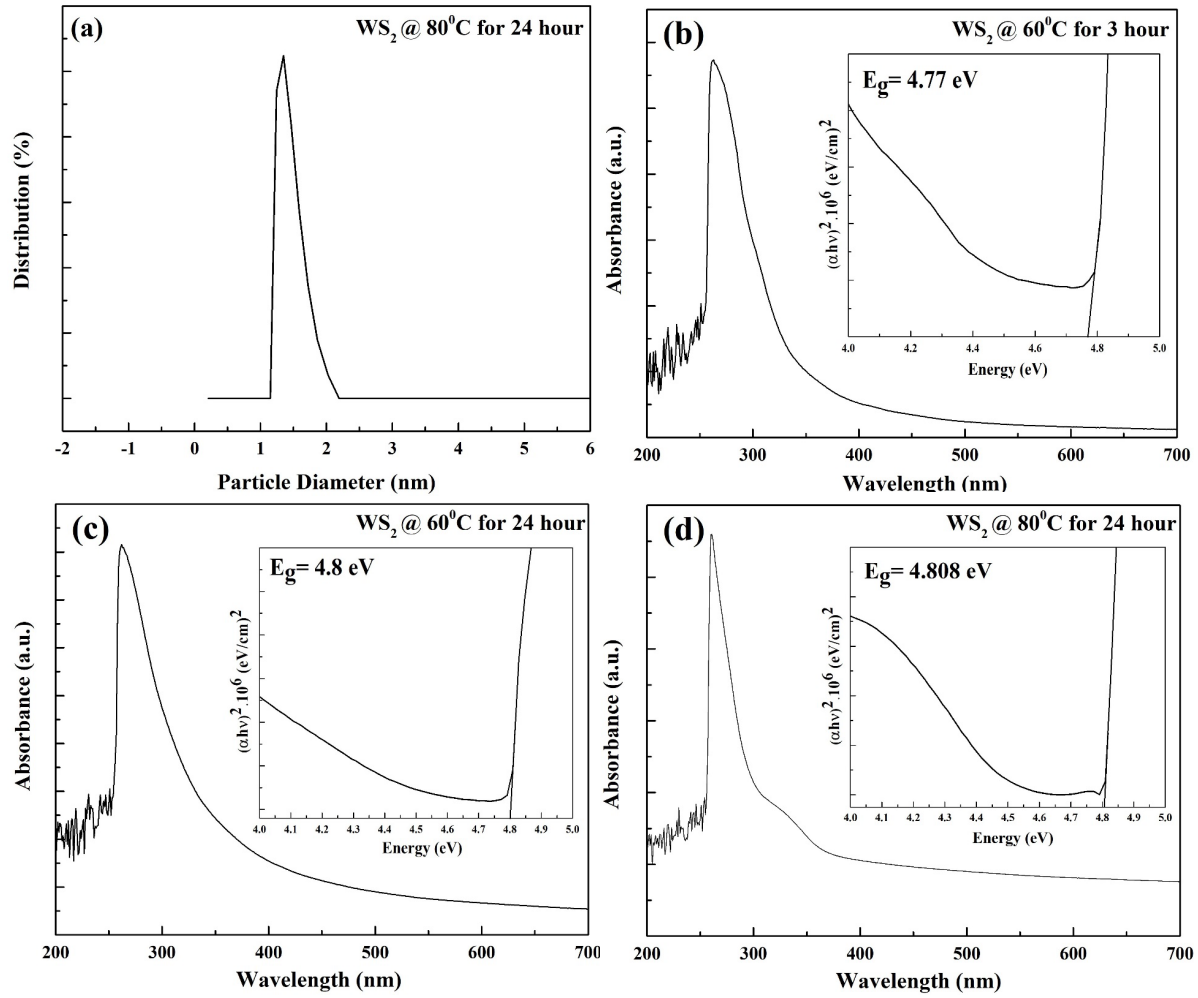


Figure 4: (a) DLS spectra obtained for the WS_2 QD sample dried at 80 °C for 24 hours. (b), (c), and (d) The UV-Vis spectra and Tauc's plot of the samples dried at 60 °C and 80 °C with varied dwelling time and particle size graph 3 hours and 24 hours.

excitons at room temperature. The A and B exciton have their origins due to the optically addressable spin-polarized valleys (±K points) in WS_2 material. The spatial confinement in the QDs samples result in a spin orbit splitting of 400 meV, calculated form the energy difference between A and B exitonic transition peaks of PL spectra, which was in accordance with the values reported in literature [13]. The origin of the third and fourth peak can be related to the localized excitons at the defect levels due to chalcogen vacancy. The chalcogen vacancy defects are the prominent defects in the WS_2 material due to their ease of formation (in terms of energy) and was reported to induce shallow donor levels at energies 0.1 to 0.3 eV below the minimum of the conduction band in monolayer WS_2 [14]. The transition at 462 nm (third peak) and 520 nm (fourth peak) can plausibly be related to the transitions from the defect related in gap state to the dispersive valence band state at the ±K point. Similar kind of excitonic features due to defect levels has been observed by Bora et al. in WS_2 QDs [15]. The energy difference between the defect bound excitons (X_1 and X_2) was about few hundreds of meV which was of the same order as that of spin orbit splitting, calculated from the unbound A and B exitonic transition peaks. The above fact strengthens our designation of the third and fourth PL peak (Figure 5) to the defect bound localized excitons.

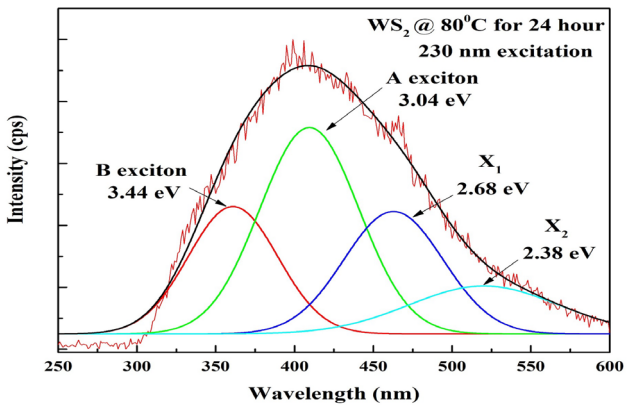


Figure 5: The PL Spectra of the WS_2 sample dried at 80 °C for 24 hours.

Conclusion

To summarize, we report a comprehensive study related to post synthesis processing of WS_2 bulk powders produced by facile solution based hydrothermal route. The physical property of the WS_2 material after drying at elevated temperature for varied dwelling time, was accessed by different techniques to understand the evolution of crystal property of

the material. Typically, it is observed that the crystal property of the hydrothermally synthesized WS_2 gets improved at elevated drying temperature. We also report a study of the optical properties of WS_2 QDs prepared by liquid phase exfoliation of dried WS_2 bulk. We observe a blueshift in the bandgap of the QDs with drying temperature and drying time and ascribed the shift because of bandgap renormalization due to transformation of the material from amorphous to crystalline state during drying process. We also evaluated the PL characteristics of the solvent dispersed WS_2 QDs and found that the emission from the material was controlled by the free (A and B) and defect bound (X_1 and X_2) excitons. Our study suggests that post synthesis drying can be an effective technique to tune the properties of WS_2 QDs which has extensive use in optoelectronic and photocatalytic applications as well as biological imaging.

Acknowledgement

The present work acknowledges the financial support from Manipal University Jaipur (MUJ) under the Enhanced Seed Grant Scheme with Project Ref. No. EF/2019-20/QE04-11. The authors acknowledge the use of PL, UV-Vis and FTIR instrument at the Sophisticated Analytical Instrument Facility (SAIF) and Central Analytical Facility (CAF), MUJ.

References

1. Reale F, Palczynski P, Amit I, Jones GF, Mehew JD, et al. 2017. High-mobility and high- optical quality atomically thin WS_2. *Sci Rep* 7(1): 14911. https://doi.org/10.1038/s41598-017-14928-2
2. Andrzejewski D, Hopmann E, John M, Kümmell T, Bacher G. 2019. WS_2 Monolayer-based light-emitting devices in a vertical p–n architecture. *Nanoscale* 11(17): 8372-8379. https://doi.org/10.1039/C9NR01573F
3. Zeng L, Tao L, Tang C, Zhou B, Long H, et al. 2016. High-responsivity UV-Vis photodetector based on transferable WS_2 film deposited by magnetron sputtering. *Sci Rep* 6(1): 1-8. https://doi.org/10.1038/srep20343
4. Afzal AM, Khan MF, Eom J. 2021. Gate-voltage-modulated spin precession in graphene/WS_2 field-effect transistors. *Electronics* 10(22): 2879. https://doi.org/10.3390/electronics10222879
5. Lan C, Li C, Ho JC, Liu Y. 2021. 2D WS_2: from vapor phase synthesis to device applications. *Adv Electron mater* 7(7): 2000688. https://doi.org/10.1002/aelm.202000688
6. Zheng Y, Sun L, Liu W, Wang C, Dai Z, et al. 2020. Tungsten oxysulfide nanosheetsfor highly sensitive and selective NH_3 sensing. *J Mater Chem C* 8(12): 4206-4214. https://doi.org/10.1039/C9TC06686A
7. Shang X, Rao Y, Lu SS, Dong B, Zhang LM, et al. 2017. Novel WS_2/WO_3 heterostructured nanosheets as efficient electrocatalystfor hydrogen evolution reaction. *Mater Chem Phys* 197: 123-128. https://doi.org/10.1016/j.matchemphys.2017.05.027
8. Perrozzi F, Emamjomeh SM, Paolucci V, Taglieri G, Ottaviano L, et al. 2017. Thermal stability of WS_2 flakes and gas sensing properties of WS_2/WO_3 composite to H_2, NH_3 and NO_2. *Sens Actuators B Chem* 243: 812-822. https://doi.org/10.1016/j.snb.2016.12.069
9. Latha M, Rani JV. 2019. WS_2/graphene composite as cathode for rechargeable aluminum-dual ion battery. *J Electrochem Soc* 167(7): 070501. https://doi.org/10.1149/2.0012007JES
10. Kumar VB, Mohanta D. 2011. Formation of nanoscale tungsten oxide structures and colouration characteristics. *Bull Mater Sci* 34(3): 435-442. https://doi.org/10.1007/s12034-011-0117-1
11. Vaziri HS, Shokuhfar A, Afghahi SSS. 2020. Synthesis of WS_2/CNT hybrid nano particles for fabrication of hybrid aluminum matrix nanocomposite. *Mater Res Express* 7(2): 025034. https://doi.org/10.1088/2053-1591/ab70e1
12. Bhatt P, Chattopadhyay S, Misra KP, Madan D, Halder N. 2021. Effect of temporal pH variation of the reaction mixture on $Mg(OH)_2$ morphology precipitated from an aqueous $Mg(NO_3)_2$-NaOH system. *Adv Powder Technol* 32(7): 2289–2299. https://doi.org/10.1016/j.apt.2021.05.002
13. Zhu ZY, Cheng YC, Schwingenschlögl U. 2011. Giant spin-orbit-induced spin splitting in two-dimensional transition-metal dichalcogenide semiconductors. *Phys Rev B* 84(15): 153402.
14. Zhou M, Wang W, Lu J, Ni Z, 2021. How defects influence the photoluminescence of TMDCs. *Nano Res* 14(1): 29-39. https://doi.org/10.1007/s12274-020-3037-9
15. Bora A, Mawlong LPL, Das R, Giri PK. 2020. Understanding the excitation wavelength dependent spectral shift and large exciton binding energy of tungsten disulfide quantum dots and its interaction with single-walled carbon nanotubes. *J Colloid Interface Sci* 561: 519-532. https://doi.org/10.1016/j.jcis.2019.11.027